

De-NO_x Performance and Mechanism of Mn-Based Low-Temperature SCR Catalysts Supported on Foamed Metal Nickel

Baozhong Zhu,^{a,#} Guobo Li,^{a,#} Yunlan Sun,^{*,a} Shoulai Yin,^a Qilong Fang,^a Zhaohui Zi,^a
Zicheng Zhu,^a Jiaxin Li^a and Keke Mao^a

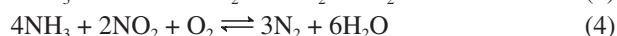
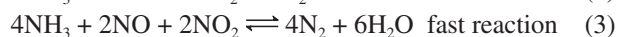
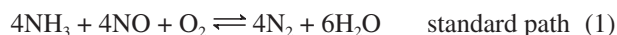
^aSchool of Energy and Environment, Anhui University of Technology,
243002 Maanshan, Anhui, P. R. China

A series of manganese-based catalysts supported on foamed metal nickel (FMN) with various Mn/Ni ratios was prepared for low-temperature selective catalytic reduction (SCR) of NO with NH₃ (NH₃-SCR). The effects of calcination temperature, amount of added Mn, optimal operating conditions, and H₂O on the elimination of nitrogen oxides (de-NO_x) performance of catalysts were studied. The catalysts were characterized by scanning electron microscopy, X-ray diffraction, X-ray photoelectron spectroscopy, and temperature-programmed desorption experiments of NH₃ analyses. The experimental results revealed that the Mn_{7.5}/FMN catalyst calcined at 350 °C exhibited the best NO conversion that was ca. 100% at 120-200 °C. Moreover, it had excellent H₂O tolerance. The superior activity of the Mn_{7.5}/FMN catalyst, which was calcined at 350 °C, was attributed to the presence of amorphous manganese oxide, more unsaturated Ni atoms and structural defects, an increase in NH₃ adsorbance, and the number of surface acid sites. Based on these studies, we established that the reaction of the NH₃-SCR with Mn_{7.5}/FMN catalyst mainly exhibits an Eley-Rideal mechanism.

Keywords: de-NO_x, low-temperature SCR, MnO_x, foamed metal nickel, mechanism

Introduction

Nitrogen oxides (NO_x) such as NO and NO₂ resulting from fossil fuel combustion are one of the main pollutants in the atmosphere. NO_x gases are responsible for acid rain, photochemical smog, and ozone layer depletion. At high levels, they affect the respiratory system, and long-term exposure can damage lung function.¹⁻³ Currently, several methods are used to eliminate NO_x (de-NO_x). Selective catalytic reduction (SCR) of NO with NH₃ (NH₃-SCR) is one of the most effective ways to reduce NO_x emissions.⁴⁻⁸ The reactions are as follows:⁵



As a core link in this technology, the catalyst performance directly affects the de-NO_x efficiency of the whole SCR system.^{9,10} The V₂O₅-WO₃ (MoO₃)/TiO₂

catalyst is a commonly used commercial SCR catalyst for NO_x removal with an active temperature range of 300-400 °C.^{11,12} However, this catalyst has many disadvantages including the toxicity of vanadium at high temperatures.¹³ Therefore, significant efforts should be devoted towards the development of non-vanadium catalysts for NH₃-SCR processes. Mn-based catalysts have been studied due to their inherent environment-friendly characteristics and excellent SCR activity at low temperatures.¹⁴⁻¹⁹ Kapteijn *et al.*²⁰ studied the single-component MnO_x catalyst and established an activity order of MnO₂ > Mn₃O₈ > Mn₂O₃ > Mn₃O₄ > MnO at a temperature range of 385-575 K. Moreover, they determined that Mn₂O₃ exhibited the highest N₂ selectivity with an NO conversion rate of ca. 100% at ca. 450 K. Wang *et al.*²¹ studied the low-temperature de-NO_x activity of MnO_x supported by multi-walled carbon nanotubes. The results revealed an activity order of manganese oxides in different valence states: MnO₂ > Mn₃O₄ > MnO, proving that the different valence states of Mn exhibit different effects on the de-NO_x activity of the catalyst.

Active coke (AC), TiO₂, and Al₂O₃ are the most widely used carriers for low-temperature SCR catalysts. Jin and

*e-mail: yunlansun@163.com

#These authors contributed equally to this work.

co-workers²² studied the low-temperature de-NO_x activity of Mn-Ce/TiO₂ and Mn-Ce/Al₂O₃ catalysts. The results indicated that the de-NO_x performance of the Mn-Ce/TiO₂ catalyst was better than that of the Mn-Ce/Al₂O₃ catalyst at temperatures of 80-150 °C. Although the Mn-based catalysts exhibit high low-temperature activities, there are significant differences in their low-temperature SCR activity.²³⁻²⁵ Moreover, the role of the carrier should not be ignored.^{26,27} Foamed metal nickel (FMN) with an excellent structure of three-dimensional all-through mesh is used as a sound absorbing “porous metal”. It exhibits a number of positive characteristics including good stability, high porosity, good thermal shock resistance, small bulk density and a large surface area, and is mainly used as a positive current collector and active carrier in nickel-based batteries.^{28,29} However, to date, few studies have concentrated on the use of FMN in the field of low-temperature de-NO_x.³⁰

In this paper, FMN is used as a de-NO_x catalyst carrier. A series of Mn-based catalysts supported on FMN with different Mn/Ni ratios were studied. The effects of calcination temperature, amount of added Mn, optimum operating conditions, and H₂O on the de-NO_x performance of the catalysts were elucidated and the mechanism was discussed.

Experimental

Catalyst preparation

Mn_x/FMN catalysts (x represents the mass ratio of Mn loading and FMN, x = 2.5, 5.0, 7.5, 10.0, 12.5, and 15.0) were prepared by the impregnation method using FMN (commercial foamed metal nickel, 98% purity) as support and manganese nitrate (50% Mn(NO₃)₂ solution) as precursor,³¹ both purchased from Sinopharm (China). A certain amount of FMN was added to the manganese nitrate solution according to the ratio of Mn and FMN. The mixture was magnetically stirred for 1 h and then dried in an oven at 105 °C for 12 h. The dried catalyst samples were subsequently calcined at 250, 350, 450, and 550 °C in a muffle furnace for 5 h. The prepared catalysts were sealed and stored until further use in subsequent experiments.

Catalytic experiments

Catalytic measurements were performed in a fixed-bed reactor using 0.3 g catalyst for each experiment.³² The simulated mixed flue gas comprised 500 ppm NO, 500 ppm NH₃, 5 vol% O₂ and was balanced with N₂. The total gas flow rate of the mixed flue gas was 100 mL min⁻¹

and the gas hourly space velocity (GHSV) was 13000 h⁻¹. A thermocouple (K-type) was used to measure the reactive temperature of the catalyst in the fixed-bed reactor. The flue gas concentrations at the inlet and outlet of the system were measured with a flue gas analyzer (ECOM J2KN, Germany). Prior to the initiation of the experiment, the simulated mixed flue gas was fed into the reactor for 0.5 h to ensure stability. Catalytic activity was evaluated from the amount of NO conversion, calculated by equation 5:

$$\eta (\%) = \frac{[\text{NO}]_{\text{in}} - [\text{NO}]_{\text{out}}}{[\text{NO}]_{\text{in}}} \times 100 \quad (5)$$

where η is the NO conversion and [NO]_{in} and [NO]_{out} indicate the NO inlet and outlet concentrations at steady state, respectively. The NO₂ concentration was negligible.

Catalyst characterization

Scanning electron microscope

A scanning electron microscope (SEM) (Hitachi S-4800, Japan) was used to investigate the microstructural features of the catalyst surface.

X-ray diffraction

X-ray diffraction (XRD) measurements were performed on an X-ray diffractometer with CuK α radiation (Bruker D8 Advance, Germany). The diffraction patterns were recorded in the 2 θ range of 10-80° at a scan speed of 10° min⁻¹ and a resolution of 0.02°.

X-ray photoelectron spectroscopy

X-ray photoelectron spectroscopy (XPS; Thermo Scientific K-Alpha spectrometer, USA) was used to study the valence state, elemental content, and energy level structure. Test conditions included an Al K α excitation source, 30 mA target current, 15 kV target voltage, a vacuum chamber pressure less than 10⁻⁷ Pa, and a 0.1 eV scan step size. The binding energies of the samples (O, Ni, and Mn) were calibrated according to contaminant carbon (C 1s = 284.6 eV).

Temperature-programmed desorption analysis of ammonia

Temperature-programmed desorption analyses of NH₃ (NH₃-TPD) were performed on Micromeritics 2920 (USA) auto-adsorption apparatus and the desorbed amount of NH₃ was also monitored by thermal conductivity detection (TCD). The 100 mg catalyst sample was placed in a reaction tube and heated to 300 °C. Next, it was pretreated under 30 mL min⁻¹ He atmosphere for 0.5 h, cooled down, and subsequently maintained at a temperature

of 80 °C. At the beginning of the adsorption process, the system was purged with a mixed gas comprising NH₃ (10 mL min⁻¹) and N₂ (30 mL min⁻¹). After adsorption was saturated, the system was purged with He at a flow rate of 30 mL min⁻¹ until the TCD detector signal was stable. Finally, the temperature was raised from 100 to 700 °C under He atmosphere (30 mL min⁻¹) and the working curve was recorded.

Results and Discussion

Evaluation of catalytic activity

Effects of calcination temperature and Mn loading on catalytic activity

Figure 1a illustrates the NO conversion percentage values of catalysts with different Mn loadings at 120-240 °C. For FMN, the conversions were basically zero at 120-240 °C, indicating its low catalytic activity. NO conversion first increased and then decreased with increasing Mn loading, which reached a maximum at a Mn loading of 7.5% and was ca. 100% at 120-200 °C. A small amount of Mn loading provides less active site and so the activity of the Mn_x/FMN catalyst is low. On the other hand, a high amount of Mn loading may cause agglomeration of the active component that in turn deteriorates the catalytic activity. The Mn loading of 7.5% is suitable, so we further studied the Mn_{7.5}/FMN catalyst.

The NO conversion activity of the Mn_{7.5}/FMN catalyst uncalcined and calcined at 250-550 °C is presented in Figure 1b, indicating that the calcination temperature had great influence on the NO_x conversion. The NO conversion activity of the Mn_{7.5}/FMN catalyst firstly increased and then decreased with the rise of calcination temperature. The Mn_{7.5}/FMN catalyst exhibited the highest activity at

a calcination temperature of 350 °C. The NO conversions were ca. 100% at 120-220 °C. Many factors may be responsible for the high NO conversions, such as surface area and surface acidity of catalyst.^{33,34} We will conduct comprehensive studies in our future work.

Effects of the NH₃/NO ratio and O₂ concentration on catalytic activity

NH₃ plays an important role in the NH₃-SCR reaction and is usually adsorbed onto the catalyst surface where it reacts with NO. Excess NH₃ molecules may result in secondary pollution in the NH₃-SCR reaction and thus, it is necessary to understand the effect of the NH₃/NO ratio on catalytic activity. Figure 2a demonstrates the effect of different NH₃/NO ratios on the NO conversion activities of the Mn_{7.5}/FMN catalyst calcined at 350 °C. At an NH₃/NO ratio < 0.8, NO conversion increased linearly with an increase in NH₃/NO ratio. According to reaction 1, it can be known that the amount of NH₃ was not enough, so the NO conversion increased linearly with an increase in NH₃/NO ratio. However, when the NH₃/NO ratio reached 1.0, the NH₃ reacted on NO completely, and thus the conversion activity became stable even increasing the amount of NH₃.

In NH₃-SCR, both O₂ and NO have oxidative capacity and thus, the oxidation reaction at the catalyst surface is a very critical step.³⁵ Hence, it is essential to study the effect of O₂ concentration on the catalytic activity. Figure 2b demonstrates that although the NO conversion of the Mn_{7.5}/FMN catalyst is only ca. 20% at an O₂ concentration of 0 ppm, it increases rapidly with an increase in O₂ concentration until it becomes stable at a concentration of ca. 1%. This indicates that the O₂ molecules participate in the reaction and the adsorbed and lattice oxygen molecules on the catalyst surface are formed rapidly,

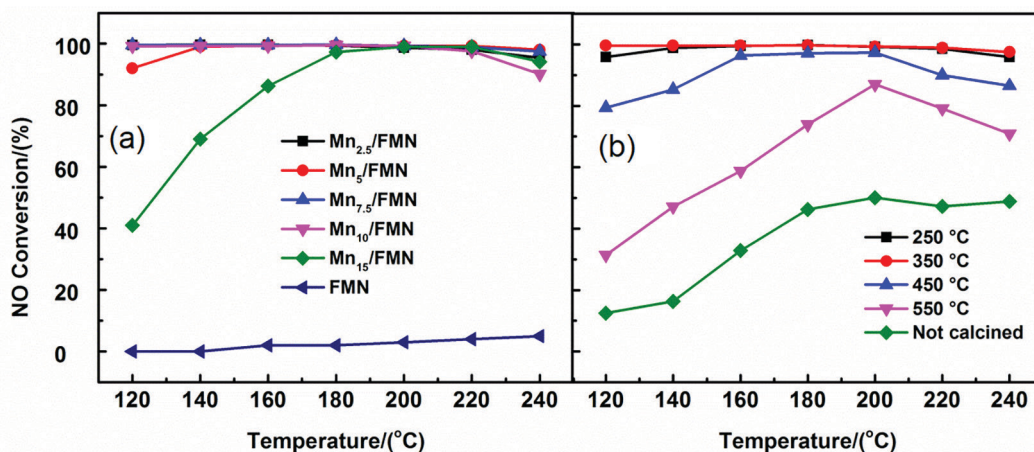


Figure 1. NO conversion activities of (a) Mn_x/FMN catalysts with different Mn loadings calcined at 350 °C and (b) Mn_{7.5}/FMN catalyst uncalcined and calcined at different temperatures. Reaction conditions: 500 ppm NO, 500 ppm NH₃, 5 vol% O₂, balanced with N₂.

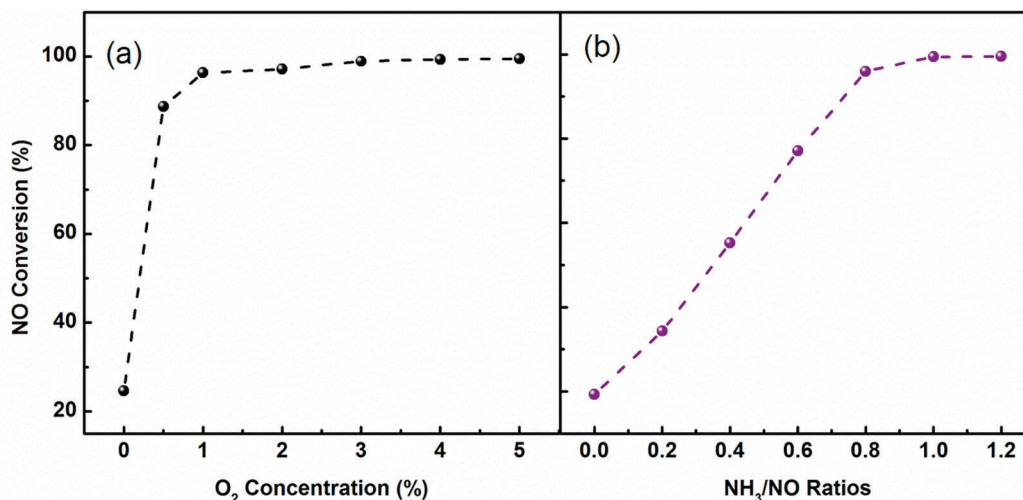


Figure 2. Effects of (a) different NH_3/NO ratios and (b) O_2 concentrations on the NO conversion activity of the $\text{Mn}_{7.5}/\text{FMN}$ catalyst calcined at 350°C . Reaction conditions: 500 ppm NO, 0-500 ppm NH_3 , 0-5 vol% O_2 , balanced with N_2 .

thereby increasing NO conversion. When the adsorbed and lattice oxygen molecules on the catalyst surface reach the saturation point (ca. 1%, Figure 2b), NO conversion remains stable, even if the O_2 concentration increases. This further explains why the oxidation capacity of O_2 on the catalyst surface is much stronger than that of NO and why the importance role of O_2 in the NH_3 -SCR reaction cannot be ignored.

Effect of H_2O on catalytic activity

H_2O has an inhibition effect on the NH_3 -SCR of NO.³⁶⁻³⁸ To investigate whether the $\text{Mn}_{7.5}/\text{FMN}$ catalyst is affected by H_2O , an H_2O resistance test was carried out at 180°C . Figure 3 displays the effect of H_2O on the NO conversion activity of the $\text{Mn}_{7.5}/\text{FMN}$ catalyst. Notably, the $\text{Mn}_{7.5}/\text{FMN}$ catalytic activity was not affected by H_2O , even at 10 vol%. In the presence of H_2O , the H_2O and NH_3 molecules compete for the active sites on the catalyst.³⁹ However, the $\text{Mn}_{7.5}/\text{FMN}$ catalyst exhibits superior H_2O resistance, indicating that the $\text{Mn}_{7.5}/\text{FMN}$ catalytic activity can be ascribed to the strong adsorption of the NH_3 molecules present on the acid sites of the catalyst.

Adsorption performance of the catalyst

To understand the adsorption characteristics of NH_3 on the surface of $\text{Mn}_{7.5}/\text{FMN}$ catalyst, the transient response characteristics of NH_3 were studied at 180°C . Figure 4a presents the changes of NO conversion activity under different conditions. In the presence of NH_3 , NO conversion reaches ca. 100% during the first stage, indicating that the more active NH_3 species existing on the $\text{Mn}_{7.5}/\text{FMN}$ catalyst surface can participate in the NO reduction reaction. When the NH_3 flow is switched off, NO conversion

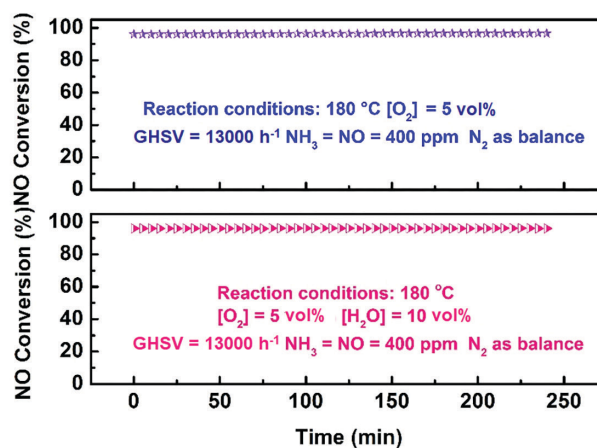


Figure 3. Effect of H_2O on the NO conversion of the $\text{Mn}_{7.5}/\text{FMN}$ catalyst. Reaction conditions: 500 ppm NO, 500 ppm NH_3 , 5 vol% O_2 , 10 vol% H_2O balanced with N_2 .

rapidly decreases until it stabilizes after half an hour. NO conversion rate is only 10%, suggesting that NO reacts with O_2 to produce nitrates and nitrites that are deposited on the catalyst surface, thus, the catalyst maintains lower NO conversion activity.⁴⁰ When NH_3 is reintroduced into the reaction system, NO conversion rapidly increases and reaches a value close to the original after ca. 10 min. It then increases slowly because the adsorbed NH_3 must first react with the nitrate that deposits onto the catalyst surface to regain the active site.⁴¹ Finally, NO conversion returns to the original value and remains stable. The NH_3 desorption time is therefore longer than its adsorption time, indicating strong adsorption onto the catalytic surface. The reaction cannot occur when NH_3 and NO are in the gas phase.⁴² If the reaction of NO with NH_3 occurs, the latter, which should be in the adsorption state, would react with NO. Figure 4a illustrates that the NH_3 desorption rate is lower than its adsorption rate, indicating that NH_3 can be adsorbed

onto the Lewis acid or Brønsted acid sites present on the catalytic surface.^{43,44}

The transient response characteristics of NO were also studied at 180 °C. Figure 4b presents the changes of NO concentration and conversion under different conditions. When the NO flow was cut off, the NO concentration dropped from 500 to 0 ppm in ca. 20 min and the NO conversion also decreased. When NO was added back to the reaction system, the NO concentration rapidly (in ca. 20 min) returned to the initial level (500 ppm), indicating that the NO adsorption capacity on the Mn_{7.5}/FMN catalyst surface is relatively weak. However, this does not imply that NO cannot be adsorbed onto the catalyst surface. Figure 4b illustrates that the catalyst exhibits high NO conversion activity, indicating that it is capable of adsorbing NO.

SEM analysis

The morphology and structure of the FMN, Mn_{7.5}/FMN and Mn₁₅/FMN catalysts were studied by SEM. The surface of FMN is very smooth and it provides an interconnected porous framework that serves as a support for the active

MnO_x species distributed on the catalyst surface (Figure 5). The surfaces of Mn_{7.5}/FMN and Mn₁₅/FMN catalysts are much rougher than that of FMN, indicating that the MnO_x species was loaded on the FMN surface. These rough surfaces can easily adsorb a large amount of gas and, thus, the activity of the catalyst increases. Notably, the surface of the Mn_{7.5}/FMN catalyst is rougher than that of Mn₁₅/FMN catalyst, indicating that the excess amount of MnO_x loaded can lead to the agglomerate of active substance.

XRD analysis

The overall crystal structure and phase purity of the Mn_x/FMN catalysts were verified by XRD. The XRD patterns of the different catalysts calcined at 350 °C are illustrated in Figure 6a. The diffraction peaks at 44.7, 52.0 and 76.5° are ascribed to the Ni from the FMN substrate in the FMN, Mn_{2.5}/FMN, Mn_{7.5}/FMN, Mn₁₀/FMN, and Mn₁₅/FMN catalysts (Figure 6a). Only the Ni diffraction peaks were detected and the absence of manganese oxide diffraction peaks was attributed to the amorphous character of manganese oxides.

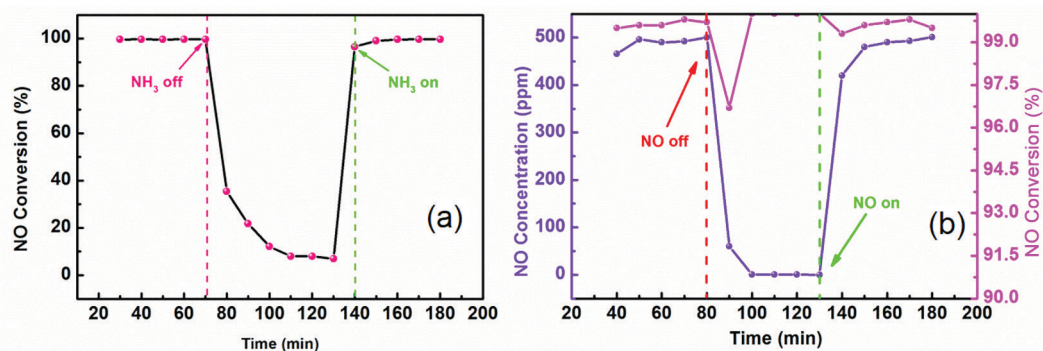


Figure 4. NH₃ (a) and NO (b) transient response curves for Mn_{7.5}/FMN catalyst calcined at 350 °C. Reaction conditions: 500 ppm NO, 500 ppm NH₃, 5 vol% O₂, balanced with N₂.

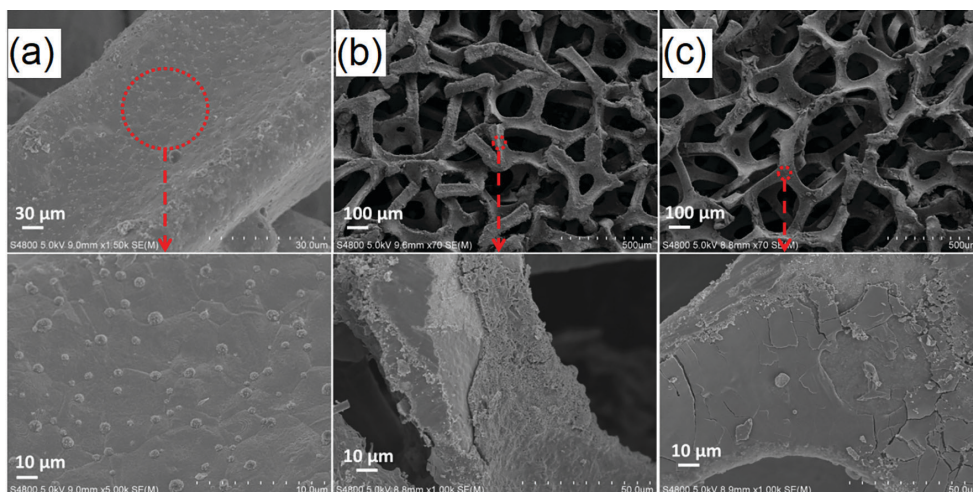


Figure 5. SEM of (a) FMN, (b) Mn_{7.5}/FMN and (c) Mn₁₅/FMN catalysts calcined at 350 °C.

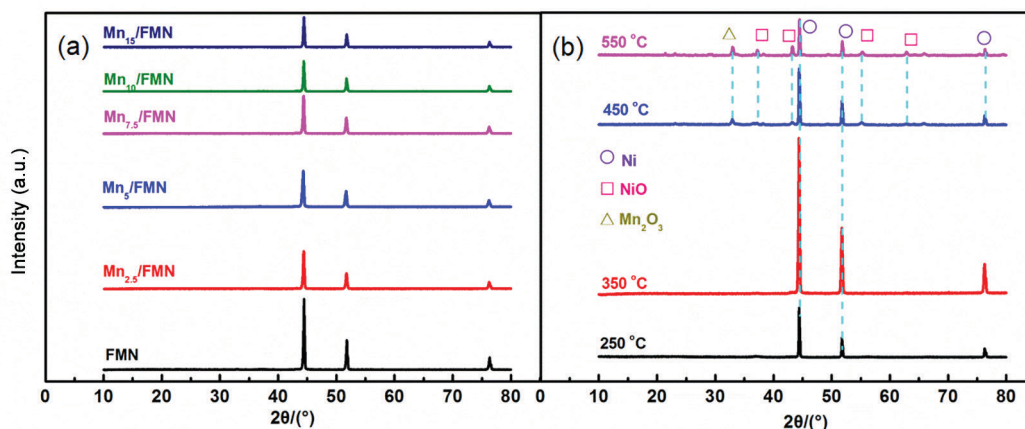


Figure 6. X-ray diffraction patterns of (a) various catalysts calcined at 350 °C and (b) the $Mn_{7.5}/FMN$ catalyst calcined at different temperatures (250, 350, 450 and 550 °C).

Figure 6b presents the X-ray diffraction patterns of the $Mn_{7.5}/FMN$ catalyst calcined at different temperatures. Only the Ni diffraction peaks were detected at calcination temperatures of 250 and 350 °C, indicating the presence of amorphous manganese oxides on the surface of the $Mn_{7.5}/FMN$ catalyst. When the calcination temperature reached 450 °C, NiO diffraction peaks were detected at 37.3, 43.3, 55.5, and 62.8° (JCPDS card No. 44-1159), while an α - Mn_2O_3 diffraction peak appeared at 33.1°. This indicates that part of the Ni was oxidized and the amorphous manganese oxides partially transformed into α - Mn_2O_3 . As the calcination temperature increased further, the intensity of the Ni diffraction peaks decreased, while that of the NiO and α - Mn_2O_3 peaks increased. This suggests that NiO and α - Mn_2O_3 formations increase with an increase in temperature. The activity of the $Mn_{7.5}/FMN$ catalyst calcined at 250 and 350 °C was higher than that at 450 and 550 °C (Figure 1b), indicating that for this catalyst, the afforded NiO and α - Mn_2O_3 exhibit an inhibitory effect on the NO conversion activity of the $Mn_{7.5}/FMN$ catalyst.

XPS analysis

XPS measurements were used to determine the atomic ratios and the valences of the surface components.

Figure 7 displays the O 1s and Ni 2p_{3/2} XPS spectra of the FMN and $Mn_{7.5}/FMN$ catalysts calcined at 350 °C. The O 1s spectrum was fitted with two characteristic peaks at ca. 529.23 and 530.90 eV ascribed to lattice oxygen (O_α) and surface-adsorbed oxygen (O_β), respectively. Notably, O_α exhibits a higher activity in the redox reaction than O_β , thereby promoting NO oxidation and simultaneously accelerating the “fast SCR” reaction.^{45,46} Therefore, a study of $O_\alpha / (O_\alpha + O_\beta)$ helps to understand the oxidation performance of the catalyst. Similarly, Ni 2p_{3/2} spectra were fitted with three characteristic peaks at ca. 853.55, 856.45, and 860.67 eV, ascribed to the main peak and two satellite peaks (represented as sat I and sat II), respectively. Sat I corresponds to Ni³⁺ species, Ni²⁺-OH species, and Ni²⁺ vacancies, while sat II was attributed to ligand-metal charge transfer.^{47,48}

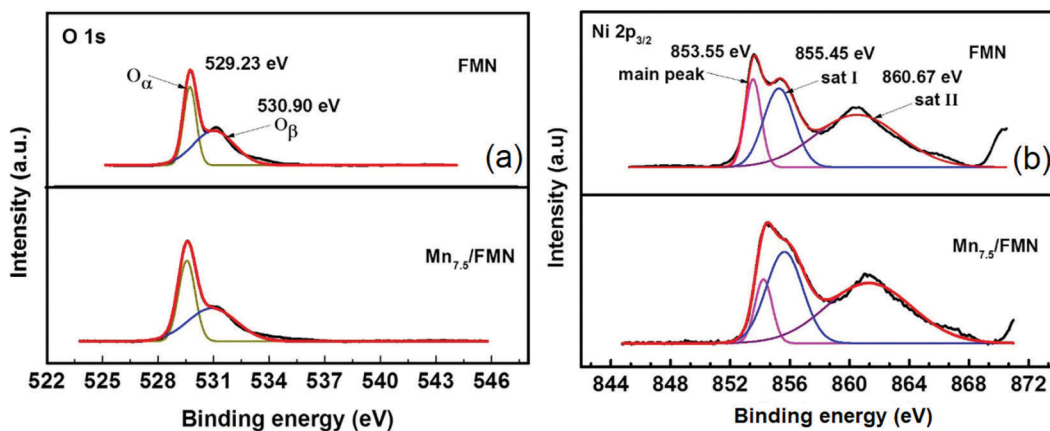


Figure 7. XPS spectra of the FMN and $Mn_{7.5}/FMN$ catalysts calcined at 350 °C: (a) O 1s and (b) Ni 2p_{3/2}.

The results afforded from the XPS analysis (Table 1) provide a better insight into the effects of each component on de-NO_x. A comparison of the results afforded by the Mn_{7.5}/FMN and FMN catalysts reveals an improvement in the sat I and sat II ratios after Mn was added. This indicates the presence of more unsaturated Ni atoms and structural defects on the surface of the Mn_{7.5}/FMN catalyst as well as interactions between the Mn and Ni atoms. In addition, the presence of O_α species is beneficial to NH₃-SCR.^{49,50} These factors contribute towards the increase in activity observed for the Mn_{7.5}/FMN catalyst.

Figure 8 presents the O 1s, Ni 2p_{3/2} and Mn 2p_{3/2} spectra for the Mn_{7.5}/FMN catalysts calcined at 350 and 550 °C. The Mn 2p_{3/2} spectra were fitted with three characteristic peaks at ca. 640.0, 642.0, and 644.2 eV, ascribed to Mn²⁺, Mn³⁺, and Mn⁴⁺, respectively.⁵¹ Mn⁴⁺ has been reported to exhibit a strong redox ability that can promote a “fast SCR” reaction.⁵² Moreover, out of all its valence states the Mn³⁺ intermediate valence state exhibits better conversion capacity and thus, it can promote the catalytic activity of the catalyst. We therefore concluded that Mn⁴⁺ and Mn³⁺ play very important roles in the low-temperature NH₃-SCR reaction.

The results from Mn_{7.5}/FMN XPS analysis are listed in Table 2. The Mn⁴⁺ and Mn³⁺ contents on the catalyst surface exhibit little change with increasing calcination temperature, however, there are significant changes in sat I and sat II. Notably, the sat I (main peak) and sat II (main peak) ratios for the Mn_{7.5}/FMN catalyst calcined at 350 °C are larger than those of the Mn_{7.5}/FMN catalyst calcined at 550 °C, illustrating that there are more unsaturated Ni atoms and structural defects on the surface of the former

catalyst. In addition, the ratio of O_α on the surface of the Mn_{7.5}/FMN catalyst calcined at 550 °C is larger than that of the Mn_{7.5}/FMN catalyst calcined at 350 °C. As discussed above (sub-section “Effects of calcination temperature and Mn loading on catalytic activity”), the Mn_{7.5}/FMN catalyst calcined at 350 °C exhibits higher activity. This indicates that the O_α ratio does not have a crucial effect on the activity of the Mn_{7.5}/FMN catalyst. For the Mn_{7.5}/FMN catalysts at different calcination temperatures, sat I and sat II play more important roles in NO conversion. Moreover, a combination of these results with the XRD results demonstrates that when the calcination temperature is raised to 550 °C, the Mn crystallinity of the Mn_{7.5}/FMN catalyst improves, while active Mn decreases. Thus, the presence of active Mn, more unsaturated Ni atoms, and structural defects on the surface of the Mn_{7.5}/FMN catalyst all contribute towards better NH₃-SCR performance.

NH₃-TPD analysis

Based on the mechanism of the NH₃-SCR reaction at low temperature, the surface acidity of the catalyst plays a very important role in the whole process.^{52,53} Thus, the acid sites on the catalyst surface were investigated via NH₃-TPD analysis. Figure 9 illustrates the NH₃-TPD profiles of the Mn_{7.5}/FMN catalyst calcined at 350 and 550 °C. The Mn_{7.5}/FMN catalyst calcined at 350 °C exhibits four distinct desorption peaks located at 127.2, 277.1, 421.1, and 645.6 °C. On the other hand, three peaks centered at 127.2, 421.1, and 645.6 °C were observed in the TPD profile of the Mn_{7.5}/FMN catalyst calcined at 550 °C. Desorption peaks at temperatures of 80-150, 150-300, and > 300 °C

Table 1. XPS results of FMN and Mn_{7.5}/FMN catalysts calcined at 350 °C

Catalyst	Sat I (main peak)	Sat II (main peak)	(O _α / O _{total}) × 100 / %
FMN	1.73	3.14	41.50
Mn _{7.5} /FMN	3.04	4.68	45.50

Sat I: Ni³⁺ species, Ni²⁺-OH species, and Ni²⁺ vacancies; sat II: ligand-metal charge transfer; O_α: lattice oxygen; FMN: foamed metal nickel.

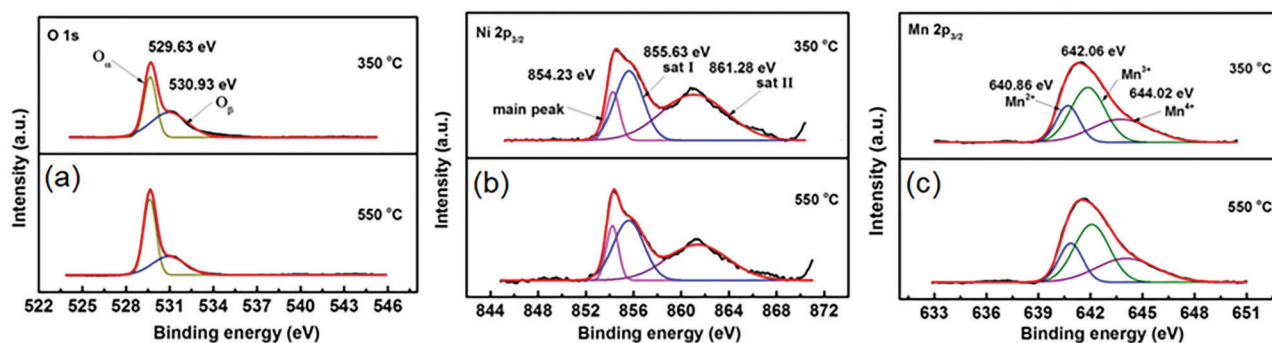


Figure 8. XPS spectra of the Mn_{7.5}/FMN catalysts calcined at 350 and 550 °C: (a) O 1s, (b) Ni 2p_{3/2}, and (c) Mn 2p_{3/2}.

Table 2. XPS results of the Mn_{7.5}/FMN catalyst calcined at 350 and 550 °C

Calcination temperature / °C	(Mn ⁴⁺ / Mn _{total}) × 100 / %	(Mn ³⁺ / Mn _{total}) × 100 / %	Sat I (main peak)	Sat II (main peak)	(O _α / O _{total}) × 100 / %
350	46.15	33.25	3.04	4.68	45.50
550	46.08	32.51	2.74	2.35	55.38

Sat I: Ni³⁺ species, Ni²⁺-OH species, and Ni²⁺ vacancies; sat II: ligand-metal charge transfer; O_α: lattice oxygen.

have been assigned to weak, medium, and strong acid sites, respectively.^{54,55} Comparison of the TPD profile of the Mn_{7.5}/FMN catalyst calcined at 350 and 550 °C suggests that the peak areas located at the weak and medium acid sites are larger for the catalyst calcined at 350 °C, while the peak areas of its strong acid sites are smaller. This indicates an increase in NH₃ adsorbance and in the number of acid sites on the surface of the Mn_{7.5}/FMN catalyst calcined at 350 °C at low temperature. Generally, more acid sites are conducive to the adsorption of reactive gases and thus, the activity of the Mn_{7.5}/FMN catalyst calcined at 350 °C is higher than that of the Mn_{7.5}/FMN catalyst calcined at 550 °C at low temperature. This demonstrates that the surface acidity plays an important role in the low-temperature NH₃-SCR reaction of the Mn_{7.5}/FMN catalyst and that NH₃ adsorption onto the weak acid sites of the Mn_{7.5}/FMN catalyst calcined at 350 °C is more favorable.

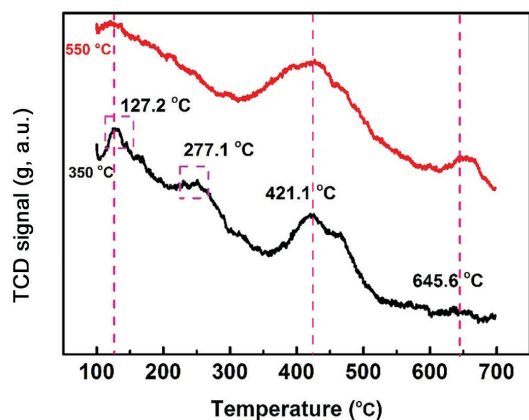


Figure 9. NH₃-TPD profiles of the Mn_{7.5}/FMN catalyst calcined at 350 and 550 °C.

NO removal mechanism

The catalytic mechanism of the Mn_{7.5}/FMN catalyst, based on the data afforded in the above mentioned studies (sections “Adsorption performance of the catalyst” and “NH₃-TPD analysis”), is presented in Figure 10. Data from the NH₃ and NO transient responses and NH₃-TPD analysis confirm that the Mn_{7.5}/FMN catalyst can adsorb NH₃ as well as adsorb NO, leading to the conclusion that the NH₃-SCR reaction of the Mn_{7.5}/FMN catalyst corresponds

to the Eley-Rideal (E-R) and Langmuir-Hinshelwood (L-H) mechanisms.^{31,56} For the E-R mechanism, the redox reaction takes place between active NH₃ and gaseous NO. The adsorbed NH₃ is activated at the weak acid site on the surface of the catalyst, with the adsorption and activation of NH₃ as the critical step. On the other hand, for the L-H mechanism, the NO of the gas phase first interacts with O₂ and subsequently the NO_x is adsorbed onto the surface of the catalyst where it is oxidized to nitrates and nitrites in the role of lattice oxygen. Finally, the adsorbed activated NH₃ reacts with the nitrates and nitrites to generate nitrogen and water. However, as discussed above (section “Adsorption performance of the catalyst”), the Mn_{7.5}/FMN catalyst adsorption capacity of NH₃ is stronger than that of NO, indicating the E-R mechanism as the main mechanism of the NH₃-SCR reaction of the Mn_{7.5}/FMN catalyst.



Figure 10. NO removal mechanism of the Mn_{7.5}/FMN catalyst.

Conclusions

A series of Mn_x/FMN catalysts were prepared by the impregnation method to study the effects of calcination temperature, amount of added Mn, optimal operating conditions, and H₂O on low-temperature NO conversion. The Mn_{7.5}/FMN catalyst calcined at 350 °C exhibited excellent NH₃-SCR activity of NO and very superior H₂O resistance. The Mn₂O₃ and NiO species were found

to exhibit a better crystallinity when the calcination temperature exceeded 350 °C. However, these species brought about a decrease in catalytic activity. The unsaturated Ni atoms, structural defects, and number of surface acid sites on the surface of the Mn_{7.5}/FMN catalyst calcined at 350 °C were greater than those of the Mn_{7.5}/FMN catalyst calcined at 550 °C. This is responsible for the excellent catalytic activity of the former catalyst. The superior H₂O resistance of the Mn_{7.5}/FMN catalyst calcined at 350 °C at low temperature can be attributed to the strong NH₃ adsorption on the acid sites. The reaction of Mn_{7.5}/FMN catalysts corresponds to both E-R and L-H mechanisms, however, the E-R mechanism plays a role in the NH₃-SCR reaction of the Mn_{7.5}/FMN catalyst.

Acknowledgments

We greatly appreciate the financial support provided by the National Natural Science Foundation of China (No. 51676001, 51376007, U1660206), the Anhui Provincial Natural Science Foundation (No. 1608085ME104), the key projects of Anhui province university outstanding youth talent (No. gxyqZD2016074, gxyqZD2017038), the Funding Projects of Back-up Candidates (No. 2017H131) and the Anhui Provincial Education Foundation (No. KJ2016A090).

References

- Skalska, K.; Miller, J. S.; Ledakowicz, S.; *Sci. Total Environ.* **2010**, *408*, 3976.
- Beirle, S.; Boersma, K. F.; Platt, U. M.; Lawrence, G.; Wagner, T.; *Science* **2011**, *333*, 1737.
- Forzatti, P.; Nova, I.; Tronconi, E.; *Angew. Chem., Int. Ed.* **2009**, *48*, 8366.
- Mou, X.; Zhang, B.; Li, Y.; Yao, L.; Wei, X.; Su, D. S.; Shen, W.; *Angew. Chem., Int. Ed.* **2012**, *51*, 2989.
- Väliheikki, A.; Kolli, T.; Huuhtanen, M.; Maunula, T.; Kinnunen, T.; Riitta, L.; Keiski, R. T.; *Top. Catal.* **2013**, *56*, 602.
- Xue, J.; Wang, X.; Qi, G.; Wang, J.; Shen, M.; Li, W.; *J. Catal.* **2013**, *297*, 56.
- Kim, Y. J.; Lee, J. K.; Min, K. M.; Hong, S. B.; Nam, I. S.; Cho, B. K.; *J. Catal.* **2014**, *311*, 447.
- Wang, D.; Zhang, L.; Li, J.; Kamasamudram, K.; Epling, W. S.; *Catal. Today* **2014**, *231*, 64.
- Li, P.; Xin, Y.; Li, Q.; Wang, Z. P.; Zhang, Z. L.; Zheng, L. R.; *Environ. Sci. Technol.* **2012**, *46*, 9600.
- Guan, B.; Zhan, R.; Lin, H.; Huang, Z.; *Appl. Therm. Eng.* **2014**, *66*, 395.
- Kompio, P. G. W. A.; Brückner, A.; Hipler, F.; Auer, G.; Löffler, E.; Grünert, W.; *J. Catal.* **2012**, *286*, 237.
- Wang, X.; Shi, A.; Duan, Y.; Wang, J.; Shen, M.; *Catal. Sci. Technol.* **2012**, *2*, 1386.
- Guo, R. T.; Wang, Q. S.; Pan, W. G.; Zhen, W. L.; Chen, Q. L.; Ding, H. L.; Yang, N. Z.; Lu, C. Z.; *Appl. Surf. Sci.* **2014**, *317*, 111.
- Yang, S.; Fu, Y.; Liao, Y.; Xiong, S.; Qu, Z.; Yan, N.; Li, J.; *Catal. Sci. Technol.* **2014**, *4*, 224.
- Zhang, R.; Yang, W.; Luo, N.; Li, P.; Lei, Z.; Chen, B.; *Appl. Catal., B* **2014**, *146*, 94.
- Boningari, T.; Smirniotis, P. G.; Thirupathi, B.; Smirniotis, P. G.; *Appl. Catal., B* **2011**, *110*, 195.
- Thirupathi, B.; Smirniotis, P. G.; *J. Catal.* **2012**, *288*, 74.
- Peña, D. A.; Uphade, B. S.; Reddy, E. P.; Smirniotis, P. G.; *J. Phys. Chem. B* **2004**, *108*, 9927.
- Ettireddy, P. R.; Ettireddy, N.; Mamedov, S.; Boolchand, P.; Smirniotis, P. G.; *Appl. Catal., B* **2007**, *76*, 123.
- Kapteijn, F.; Rodriguez-Mirasol, J.; Moulijn, J. A.; *Appl. Catal., B* **1996**, *9*, 25.
- Wang, L.; Huang, B. C.; Su, Y. X.; Zhou, G. Y.; Wang, K. L.; Luo, H. C.; Ye, D. Q.; *Chem. Eng. J.* **2012**, *192*, 232.
- Yu, G. F.; Wei, Y. F.; Jin, R. B.; Zhu, H.; Gu, Z. Y.; Pan, L. L.; *J. Environ. Sci.* **2012**, *32*, 1743.
- Smirniotis, P. G.; Srekanth, P. M.; Pena, D. A.; Jenkins, R. G.; *Ind. Eng. Chem. Res.* **2006**, *45*, 6436.
- Wang, L.; Huang, B.; Su, Y.; Zhou, G.; Wang, K.; Luo, H.; Ye, D.; *Chem. Eng. J.* **2012**, *192*, 232.
- Jiang, B. Q.; Liu, Y.; Wu, Z. B.; *J. Hazard. Mater.* **2009**, *162*, 1249.
- Gao, R.; Zhang, D.; Maitrad, P.; Shi, L.; Rungrotmongkol, T.; Li, H.; Zhang, J.; Cao, W.; *J. Phys. Chem. C* **2013**, *117*, 10502.
- Sultana, A.; Sasaki, M.; Hamada, H.; *Catal. Today* **2012**, *185*, 284.
- Zhang, J.; Baro, M. D.; Pellicer, E.; Sort, J.; *Nanoscale* **2014**, *6*, 12490.
- Zhang, L.; Xiong, K.; Chen, S. G.; Li, L.; Deng, Z. H.; Wei, Z. D.; *J. Power Sources* **2015**, *274*, 114.
- Yuan, C.; Wu, H. B.; Xie, Y.; Lou, X. W.; *Angew. Chem., Int. Ed.* **2014**, *53*, 1488.
- Lin, Z.; Lei, Z.; Qu, H. X.; Zhong, Q.; *J. Mol. Catal. A: Chem.* **2015**, *409*, 207.
- Chen, J.; Zhu, B.; Sun, Y.; Yin, S.; Zhu, Z.; Li, J.; *J. Braz. Chem. Soc.* **2018**, *29*, 79.
- Wang, J. H.; Dong, X. S.; Wang, Y. J.; Li, Y. D.; *Catal. Today* **2015**, *245*, 10.
- Yoon, D. Y.; Park, J. H.; Kang, H. C.; Kim, P. S.; Nam, I. S.; Yeo, G. K.; Kil, J. K.; Cha, M. S.; *Appl. Catal., B* **2011**, *101*, 275.
- Bosch, H.; Janssen, F. J. G.; Kerkhof, F. M. G. V. D.; Jaap, O.; Jan, G. V. O.; Julian, R. H. R.; *Appl. Catal.* **1986**, *25*, 239.
- Liu, F. D.; He, H.; Lian, Z. H.; Shan, W. P.; Xie, L. J.; Asakura, K.; Yang, W. W.; Deng, H.; *J. Catal.* **2013**, *307*, 340.

37. Huang, Z.; Liu, Z.; Zhang, X.; Liu, Q.; *Appl. Catal., B* **2006**, *63*, 260.
38. Hu, P. P.; Huang, Z. W.; Hua, W. M.; Gu, X.; Tang, X. F.; *Appl. Catal., A* **2012**, *437-438*, 139.
39. Turco, M.; Lisi, L.; Pirone, R.; Ciambelli, P.; *Appl. Catal., B* **1994**, *3*, 133.
40. Si, Z. C.; Weng, D.; Wu, X. D.; Ma, Z. R.; Ma, J.; Ran, R.; *Catal. Today* **2013**, *201*, 122.
41. Kijlstra, W. S.; Brands, D. S.; Smit, H. I.; Bliiek, A.; *J. Catal.* **1997**, *171*, 219.
42. Larrubia, M. A.; Ramis, G.; Busca, G.; *Appl. Catal., B* **2000**, *27*, 145.
43. Lin, S. D.; Gluhoi, A. C.; Nieuwenhuys, B. E.; *Catal. Today* **2004**, *90*, 3.
44. Chen, T.; Guan, B.; Lin, H.; Zhu, L.; *Chin. J. Catal.* **2014**, *35*, 294.
45. Zhao, B.; Ke, X. K.; Bao, J. H.; Wang, C. L.; Dong, L.; Chen, Y. W.; Chen, H. L.; *J. Phys. Chem. C* **2009**, *113*, 14440.
46. Zhang, L.; Zhang, D. S.; Zhang, J. P.; Cai, S. X.; Fang, C.; Huang, L.; Li, H. R.; Gao, R. H.; Shi, L. Y.; *Nanoscale* **2013**, *5*, 9821.
47. Zhao, B.; Ke, X. K.; Bao, J. H.; Wang, C. L.; Dong, L.; Chen, Y. W.; Chen, H. L.; *J. Phys. Chem. C* **2010**, *113*, 14440.
48. Cai, S. X.; Zhang, D. S.; Shi, L. Y.; Xu, J.; Zhang, L.; Huang, L.; Li, H. R.; Zhang, J. P.; *Nanoscale* **2014**, *6*, 7346.
49. Liu, F. D.; He, H.; *J. Phys. Chem. C* **2010**, *114*, 16929.
50. Shan, W.; Liu, F.; He, H.; Shi, X.; Zhang, C.; *Chem. Commun.* **2011**, *47*, 8046.
51. Pena, D. A.; Uphade, B. S.; Smirniotis, P. G.; *J. Catal.* **2004**, *221*, 421.
52. Liu, Y.; Xu, J.; Li, H. R.; Cai, S. X.; Hu, H.; Fang, C.; Shi, L. Y.; Zhang, D. S.; *J. Mater. Chem. A* **2015**, *3*, 11543.
53. Xu, L.; Li, X. S.; Crocker, M.; Zhang, Z. S.; Zhu, A. M.; Shi, C.; *J. Mol. Catal. A: Chem.* **2013**, *378*, 82.
54. Roy, S.; Viswanath, B.; Hegde, M. S.; Madras, G.; *J. Phys. Chem. C* **2008**, *112*, 6002.
55. Xu, H. D.; Wang, Y.; Cao, Y.; Fang, Z. T.; Lin, T.; Gong, M. C.; Chen, Y. Q.; *Chem. Eng. J.* **2014**, *240*, 62.
56. Lin, Z.; Zhong, Z. P.; Han, Y.; Wang, C. H.; *J. Colloid Interface Sci.* **2016**, *478*, 11.

Submitted: October 20, 2017

Published online: March 8, 2018

